Title

Dissolution of 2D Molybdenum Disulfide Generates Differential Toxicity among Liver Cell Types Compared to Non-Toxic 2D Boron Nitride Effects

Journal

Small, 17(25)

ISSN

1613-6810

Authors

Li, Jiulong
Guiney, Linda M
Downing, Julia R
et al.

Publication Date

2021-06-01

DOI

10.1002/smll.202101084

Peer reviewed

HHS Public Access

Author manuscript

Small. Author manuscript; available in PMC 2022 June 01.

Published in final edited form as:

Small. 2021 June ; 17(25): e2101084. doi:10.1002/smll.202101084.

Dissolution of 2D Molybdenum Disulfide Generates Differential Toxicity among Liver Cell Types Compared to Non-Toxic 2D Boron Nitride Effects

Jiulong Li

Center of Environmental Implications of Nanotechnology (UC CEIN), California Nanosystems Institute, University of California, Los Angeles, CA 90095, USA

Linda M. Guiney, **Julia R. Downing**

Departments of Materials Science and Engineering Chemistry, and Medicine, Northwestern University, Evanston, IL 60208, USA

Xiang Wang

Center of Environmental Implications of Nanotechnology (UC CEIN), California Nanosystems Institute, University of California, Los Angeles, CA 90095, USA

Division of Nanomedicine, Department of Medicine, University of California, Los Angeles, CA 90095, USA

Chong Hyun Chang, **Jinhong Jiang**, **Qi Liu**, **Xiangsheng Liu**, **Kuo-Ching Mei**

Center of Environmental Implications of Nanotechnology (UC CEIN), California Nanosystems Institute, University of California, Los Angeles, CA 90095, USA

Yu-Pei Liao,

Division of Nanomedicine, Department of Medicine, University of California, Los Angeles, CA 90095, USA

Tiancong Ma,

Center of Environmental Implications of Nanotechnology (UC CEIN), California Nanosystems Institute, University of California, Los Angeles, CA 90095, USA

Huan Meng,

Center of Environmental Implications of Nanotechnology (UC CEIN), California Nanosystems Institute, University of California, Los Angeles, CA 90095, USA

Division of Nanomedicine, Department of Medicine, University of California, Los Angeles, CA 90095, USA

Mark C. Hersam

anel@mednet.ucla.edu, txia@ucla.edu.

Conflict of Interest

The authors declare no conflict of interest. IP developed by Dr. Nel was licensed to Westwood Bioscience and NAMMI Therapeutics by The Regents of UC. Andre E. Nel is a co-founder, equity holder, and Executive Board member in Westwood Bioscience Inc.

Supporting Information

Supporting Information is available from the Wiley Online Library or the author.

Departments of Materials Science and Engineering Chemistry, and Medicine, Northwestern University, Evanston, IL 60208, USA

André E. Nel, **Tian Xia**

Center of Environmental Implications of Nanotechnology (UC CEIN), California Nanosystems Institute, University of California, Los Angeles, CA 90095, USA

Division of Nanomedicine, Department of Medicine, University of California, Los Angeles, CA 90095, USA

Abstract

Two-dimensional (2D) boron nitride (BN) and molybdenum disulfide (MoS_2) materials are increasingly being used for applications due to novel chemical, electronic and optical properties. Although generally considered biocompatible, recent data have shown that BN and MoS_2 could be potentially hazardous under some biological conditions, e.g., during, biodistribution of drug carriers or imaging agents to the liver. However, the effects of these 2D materials on liver cells such as Kupffer cells (KCs), liver sinusoidal endothelial cells (LSECs), and hepatocytes, are unknown. Here, we compared the toxicity of BN and MoS_2, dispersed in Pluronic F87 (designated BN-PF and MoS_2-PF) with aggregated forms of these materials (BN-Agg and MoS_2-Agg) in liver cells. MoS_2 induced dose-dependent cytotoxicity in KCs, but not other cell types, while the BN derivatives were non-toxic. The effect of MoS_2 could be ascribed to nanosheet dissolution and the release of hexavalent Mo, capable of inducing mitochondrial ROS generation and caspases 3/7-mediated apoptosis in KUP5 cells. In addition, the phagocytosis of MoS_2-Agg triggered an independent response pathway involving lysosomal damage, NLRP3 inflammasome activation, caspase-1 activation, IL-1β and IL-18 production. These findings demonstrate the importance of Mo release and the state of dispersion of MoS_2 in impacting Kupffer cell viability.

Graphical Abstract

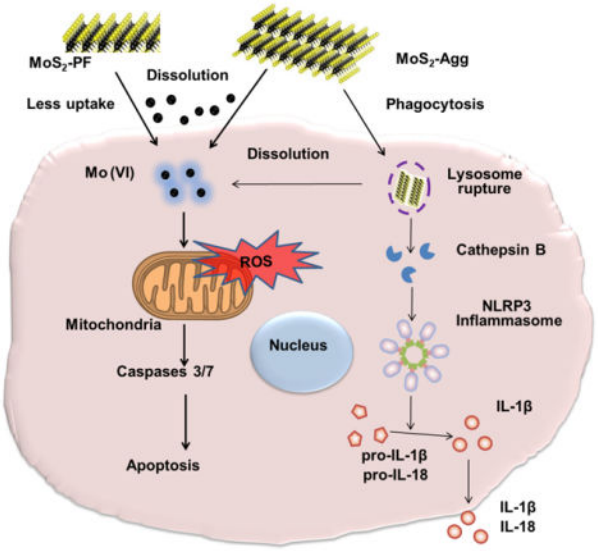

MoS_2 induces different cytotoxicity in KCs, LSECs, and hepatocytes. The well-dispersed MoS_2-PF demonstrates minimal cellular uptake, but the released Mo (VI) induces ROS generation,

caspase 3/7 activation, and apoptosis in KCs. For MoS_2-Agg phagocytized by KCs, its intracellular and extracellular dissolution also induces apoptosis. Additionally, the phagocytized MoS_2-Agg triggers lysosomal rupture, cathepsin B release, caspase-1 activation, and IL-1β production.

Keywords

boron nitride; molybdenum disulfide; dissolution; apoptosis; inflammatory response

1. Introduction

Two-dimensional (2D) nanomaterials are increasingly being used for commercial applications in the fields of energy generation, sensors, catalysis, electronics, and biomedicine, based on attractive physicochemical attributes such as their atomically thin layer structure with high surface area and free surface energy levels.[1,2] Molybdenum disulfide (MoS_2) is representative of a prototypical 2D transition metal dichalcogenide (TMD), which consists of a molybdenum sheet bonded on both sides by sulfur layers.[3,4] Not only does MoS_2 allow excellent control of 2D film thickness, but is also characterized by high electrochemical activity, excellent light-heat conversion, carrier transport efficacy, and single-photon and two-photon fluorescence imaging properties.[5] These attributes allow the frequent use of MoS_2 for applications in the fields of electronics,[6,7] composites,[8] drug delivery,[9] therapy,[10] bio-sensing, and bio-imaging.[11,12]

Hexagonal boron nitride (BN), a graphene structural analog, is another popular layered material with exceptionally high chemical and thermal stability, flexibility, elasticity, and good biocompatibility due to the hexagonal arrangement of the boron and nitrogen atoms in the 2D material lattice.[13–16] Accordingly, BN has kindled interest for thermal management,[17,18] use of its dielectric properties as a support material for bone engineering and drug delivery.[19,20]

Although BN and MoS_2 are generally considered as biocompatible materials, several studies have shown that the dissolution properties of these materials can be associated with adverse cellular responses under some circumstances.[21] For example, Liu *et al.* have shown that BN and MoS_2 nanoflakes can decrease the cell viability of human hepatoma cells because of the release of soluble boron (B) and Mo species.[22] Moreover, Li *et al.* reported that hollow BN nanospheres could increase apoptotic cell death in prostate cancer cells due to B release.[23] The liver serves as a primary sequestration site for nanoparticles that gain access to the systemic circulation from the primary site of material deposition or direct injection into the bloodstream.[24] Accordingly, it has been shown during drug carrier applications for BN or MoS_2 that sequestration in the liver needs to consider possible adverse effects in this organ.[25,26] For instance, Yu *et al.* have demonstrated the development of localized liver lesions in adult zebrafish during exposure to dispersible MoS_2 micro-sheets.[27] However, the mechanism of liver toxicity at the molecular level is still unclear and there has been no attempt to differentiate between the adverse impact on specific liver cell types. This stresses the importance of understanding the differential effects of BN or MoS_2 on specific liver cell

types that may encounter the 2D materials that are being delivered to liver sinusoids from hepatic and portal blood circulations.

One approach for elucidating the impact of 2D BN or MoS_2 nanomaterials on the liver is to compare their effects on Kupffer cells (KCs), liver sinusoidal endothelial cells (LSECs), and hepatocytes. The Kupffer cell is a major component of the mononuclear phagocyte system (MPS), which makes up 15% of all liver cells and 80−90% of all body tissue macrophages.[28] Moreover, these cells play a central role in the phagocytosis of particulate materials, modulation of innate immune responses, and endotoxin removal.[24,28–30] KCs also provide the first line of defense against nanoparticles entering the systemic circulation.[24,31,32] Although it has been shown that MoS_2 and boron nitride nanotubes induce cell stress or pro-inflammatory effects in human macrophages,[33–35] no systematic studies have been performed to address the effects of BN or MoS_2 nanosheets on KCs. In our previous studies looking at the impact of a variety of metal oxide (MOx) and rare earth oxide (REO) nanoparticles on Kupffer cells, we have demonstrated the utility of the immortalized Kupffer cell line, KUP5, in providing a good readout of the toxic potential of nanomaterials on primary KC responses.[36] In the case of LSECs, these cells also make an important contribution to the function of the reticuloendothelial system. Although only representing ~3% of all liver cell types, LSECs occupy a total surface area of ~200 m^2 in a human adult.[37] LSECs participate in particle uptake by clathrin-mediated endocytosis and play a major role in clearing blood-borne waste products and the regulation of innate immune responses.[38–40] Although transferrin-bound BN has been shown to decrease the viability of human umbilical vein endothelial cells, while PVP-coated MoS_2 nanoparticles were capable of protecting human aortic endothelial cells from oxidative stress responses,[41,42] no toxicity studies have been carried out on these materials in liver endothelial cells. However, we did demonstrate that the immunoregulatory effects of antigen-encapsulating PLGA nanoparticles on LSECs *in vivo* are mimicked by the impact of these tolerogenic nanoparticles on SV40-immortalized mouse hepatic sinusoidal endothelial cell line.[43] Hepatocytes, which comprise 60–80% of all liver cells, perform important metabolic, endocrine, and secretory functions.[24,40] While the impacts of BN or MoS_2 on hepatocytes have been assessed in previous studies, the data have been conflicting. Thus, while Liu *et al.* have demonstrated BN and MoS_2 toxicity in human HepG2 hepatocytes,[22] Li *et al.* and Sobańska *et al.* failed to show toxicity in hepatocytes, even after high-dose exposures over prolonged periods.[44,45] One possible explanation is that differences in the physicochemical properties of the BN or MoS_2 study materials could affect their structure-toxicity relationships. This has been demonstrated in a study in which we looked at the impact of MoS_2 on the lung, where the dispersion status of the material was critical in determining pulmonary toxicity.[33]

Wang *et al.* have previously reported that aggregated MoS_2 induces acute pro-inflammatory and pro-fibrogenic effects in the lung compared to lack of toxicity when the material was dispersed in Pluronic F87 or exfoliated by Li.[33] To assess the effects of BN and MoS_2 nanosheets on liver cells, we established a nanomaterial library that included dispersed and aggregated BN and MoS_2 nanosheets. Pluronic-dispersed BN (BN-PF) and MoS_2 (MoS_2-PF) were prepared by immersing the BN and MoS_2 powders in a Pluronic F87 solution, allowing aggregated materials to be collected by flocculation and filtration, leaving the

dispersed materials in the supernatant. This allowed us to compare the possible adverse effects of these materials on KUP5, SV40-transformed murine LSECs, and Hepa 1–6 cell lines. Nanoparticle toxicity in liver cells can be mainly attributed to the generation of programmed cell death (or apoptosis), which involves activation of caspases 3 and 7, or the generation of pyroptosis, which involves the activation of caspase 1 by a pathway that is triggered by lysosomal damage. While cellular apoptosis can lead to membrane blebbing, accompanied by nuclear condensation, pyroptosis is characterized by giant cell blebbing, with an increase in cell size.[33,36] We demonstrate a major impact of MoS_2 dissolution in inducing oxidative stress-mediated apoptotic death in KUP5, but not other cell types. We also observed that aggregated MoS_2 could trigger a cellular pathway in KUP5 cells, leading to NLRP3 inflammasome activation and IL-1β production.

2. Results

2.1 Physicochemical Characterization and Abiotic Assessment of Aggregated and Dispersed BN and MoS_2 Materials

Two-dimensional BN and MoS_2 nanomaterials were prepared as aggregated or dispersed nanosheets, using the ultrasonication, flocculation, filtration, washing, and resuspension procedures, outlined in the methods section. Comprehensive physicochemical characterization of these materials is detailed in Figure 1. Atomic force microscopy (AFM) revealed that, compared to the micron-scale dimensions of BN-Agg that requires scanning electron microscopy (SEM) viewing (Figure S1), Pluronic-dispersed BN exhibited sheet-like structures that display an average square root surface area of 86 ± 59 nm and average thickness of 10.4 ± 9.3 nm (Figure 1A). While the SEM analysis of MoS_2-Agg also showed large or aggregated structures, MoS_2-PF showed nanosheets with an average square root surface area of 56 ± 28 nm and an average thickness of 3.5 ± 1.9 nm (Figure 1B).

X-ray photoelectron spectroscopy (XPS) was used to confirm the chemistry of the BN and MoS_2 samples. Figure 1C shows 1s core-level spectra for the boron (B) atom in BN-Agg and BN-PF, where the main peak at 190.4 eV represents B−N bonding, with the smaller peak at 191.7 eV representative of B−O bonds.[46] This shows similar levels of oxidation for BN-Agg (10.6 ± 2.2%) and BN-PF (11.4 ± 2.5%) (Table 1). Regarding the 1s nitrogen (N) atom spectrum, the two peaks at 398.0 and 399.1 eV represent N−B and N−H bonds, respectively.[46] Figure 1D shows the Mo atom 3d and S-2p spectra for the MoS_2-Agg and MoS_2-PF samples. In addition, the peak at 226.4 eV represents the S-2s orbital, while peaks at 229.3 eV and 232.4 eV reflect the doublet of Mo (IV) 3d5/2 and 3d3/2 orbitals, respectively.[47] The fitted curves of the doublet peak at 233.4 eV and 236.0 eV corresponds to the Mo (VI) 3d5/2 and 3d3/2, respectively.[48] Moreover, the S_2^- peaks at S-2p1/2 (162.0 eV) and S 2p3/2 (163.3 eV) represent MoS_2 surface oxidation.[49] The increased percentage of Mo (VI) in the 3d orbital of MoS_2-PF (10.2 ± 1.4%) *vs.* the 3d orbital of MoS_2-Agg (3.3 ± 0.8%) reflects the increased oxidative status of the former material surface (Table 2).

The surface oxidation state of BN and MoS_2 will determine the redox potential of the nanosheet surfaces. To assess the ability of the BN and MoS_2 nanosheets to generate reactive oxygen species (ROS), we used the readout from a fluorogenic dye, H_2DCFDA, to perform an abiotic assay.[50] The assay included the use of ZnO nanoparticles, which induced the

most robust increase in DCF fluorescence intensity along with MoS_2-PF (Figure 1E). These responses were stronger than the effect of MoS_2-Agg, which in turn, exceeded the responses to BN-Agg or BN-PF. In addition to assessing ROS generation, we also used a luminescence-based GSH-Glo assay to assess the abiotic conversion of glutathione (GSH) to GSSG (Figure 1F). This provided a more quantitative comparison of the redox-active status of the 2D materials, showing that while the BN nanosheets exert no effect, that MoS_2-Agg and MoS_2-PF could decrease GSH levels by 7.1% and 23.5%, respectively. The difference between MoS_2-PF and MoS_2-Agg was statistically significant ($p < 0.05$).

Dynamic light scattering (DLS) was used to assess the hydrodynamic size, polydispersity index (PDI), and zeta potential of the 2D materials in DI water and cell culture media.[33,49,51] The tendency of the hydrodynamic diameter of the materials to be smaller in water than in tissue cell culture media is explained by the adsorption of fetal calf serum proteins to BN and MoS_2 surfaces.[51] The average hydrodynamic sizes of aggregated MoS_2 or BN were significantly larger than the dispersed samples in different media, particularly for BN (Table 3). Although PDI values < 0.4 are indicative of adequate dispersion, the dispersion indices for materials prepared in Pluronic F87 were considerably improved. All the nanosheets exhibited negative zeta potential values, which diminished in the presence of cell culture media, likely as a result of double-layer formation and protein absorption to the material surfaces. The use of a Limulus amebocyte lysate (LAL) assay showed endotoxin levels of ~0.6 EU/mL, which rules out significant bacterial contamination (Figure S2).

2.2 BN and MoS_2 Induce Differential Cytotoxicity in KUP5, LSECs, and Hepa 1−6 Cells

Provisional toxicological profiling was obtained in a transformed KC (KUP5), LSECs, and hepatocyte (Hepa 1−6) cell lines, using the MTS assay (Figure 2A). These results demonstrated differences in the response profiles of individual cell types, as well as among different materials, over the concentration range of 0–100 μg/mL. While BN-Agg and BN-PF failed to impact the viability of any cells, MoS_2-Agg and MoS_2-PF were significantly more toxic in KUP5 than in LSECs or Hepa 1−6 (except at 100 μg/mL for LSECs). The dose-dependent decrease in KUP5 viability was significantly higher for MoS_2-PF than MoS_2-Agg at concentrations > 50 μg/mL (Figure 2A). A visual display of the cytotoxic effects is provided by the heatmaps shown in Figure 2B, where yellow intensity development indicates significantly more toxicity than green coloration. All considered, these data show that MoS_2 toxicity differs among different cell types and that MoS_2-PF resulted in a stronger effect in KUP5 cells. To explain these differences, further biological assays were carried out to explain the mechanisms of injury in relation to the state of material dispersion, dissolution, cellular uptake, and redox potential.

2.3 Dissolution and Cellular Uptake of BN and MoS_2 Determine Cellular Toxicity

In addition to surface redox effects of 2D nanomaterials, it is known that the dissolution of BN and MoS_2 nanosheets under biological conditions can lead to the release of potentially toxic B or Mo species.[22,23,49] For example, it is known that the suspension of MoS_2 nanosheets in O_2-containing aqueous media is accompanied by oxidative dissolution, leading to the formation of MoO_4^{2-} and SO_4^{2-} ionic species (Figure 3A).[49] To assess the contribution of material dissolution to KC toxicity, supernatants were collected from BN and

MoS_2 nanosheets after suspension in DI water and DMEM medium for 0 and 24 h, followed by centrifugation at 15 000 rpm. The data obtained by inductively coupled plasma-mass spectrometry (ICP-MS) demonstrated that MoS_2 showed significantly higher dissolution than BN and that the dissolution rate of MoS_2-PF was significantly higher than MoS_2-Agg (Figure 3B). These results are consistent with the differential impact of these materials on abiotic redox activity and KUP5 cytotoxicity.

To determine the contribution of soluble Mo species to KUP5 toxicity, supernatants and pellets were collected from MoS_2-Agg and MoS_2-PF suspensions to repeat the MTS assay. This demonstrated that the supernatants were indeed toxic to KUP5 cells, and that supernatant removal could reduce the adverse impact of the MoS_2 suspensions (Figure 3C). A soluble molybdate (Na_2MoO_4) salt was used as a positive control in these experiments. The release of Mo (VI) as MoO_4^{2-} represents the relevant Mo species responsible for MoS_2 toxicity.[49,52] The higher level of Mo (VI) on the MoS_2-PF surface (Figure 1D or Table 2) as well as the higher rate of release of the hexavalent ion is responsible for the higher rate of cytotoxicity in MoS_2-PF-treated KUP5 cells.

It has been demonstrated that extra- as well as intracellular dissolution of metal and metal oxide nanoparticles as well as TMD nanosheets can contribute to nanomaterial toxicity.[22,53] Using optical microscopy to view cellular uptake, we observed significant increases in the staining intensity of KUP5, LSEC, and Hepa 1–6 cells during exposure to MoS_2-Agg, compared to MoS_2-PF, BN-PF, or BN-Agg (Figure 3D). To quantify the cellular content of Mo and B, ICP-MS was performed on KUP5, LSEC, and Hepa 1–6 cells after their incubation in each material for 16 h. The ICP-MS results demonstrated that the cellular association of Mo or B was significantly higher for exposed KUP5 cells compared to LSECs and Hepa 1–6 cells (Figure 3E). This is in agreement with the differential cytotoxicity in these cell types. Moreover, the cellular association or uptake of Mo was significantly higher than the uptake of B, which is consistent with the cytotoxicity data in KUP5 cells. Importantly, the cellular Mo content was higher for MoS_2-Agg than KUP5 cells exposed to MoS_2-PF (Figure 3E). This agrees with the higher Mo content in cells exposed to MoS_2-Agg pellets versus exposure to supernatants (Figure S3). To assess whether phagocytosis is involved in MoS_2-Agg uptake, KUP5 cells were treated with wortmannin (WM), a phagocytosis inhibitor,[54] before MoS_2-Agg exposure. Optical microscopy as well as the performance of an MTS assay, demonstrated decreased cellular uptake and cytotoxicity in the presence of WM (Figure S4). In contrast, cytochalasin D (macropinocytosis inhibitor) and pitstop 2 (blocking ligand access to the clathrin terminal domain) had no effects.

In addition to phagocytosis uptake, the internalized MoS_2-Agg was capable of triggering NRLP3 inflammasome activation through cathepsin B release, as demonstrated by the ability to induce caspase-1 activation in a confocal microscope as well as a microplate reader (Figure 4A–B and Figure S5). Gd_2O_3 nanoparticles, which are capable of generating surface-dependent lysosomal damage and cathepsin B release, was used as a positive control.[36] In contrast, MoS_2-PF and Mo (VI) had no effect. Caspase-1 activation was accompanied by increased IL-1β and IL-18 release from KUP5 cells treated with MoS_2-Agg and Gd_2O_3 (Figure 4C and Figure S6). The involvement of lysosomes was further confirmed by using bafilomycin A1 (Baf A1) (Figure 4D and S4B), which interferes in the lysosomal

acidification through the inhibition of vacuolar H^+-ATPases (V-ATPases).[55] Not only did Baf A1 interfere in IL-1β release by MoS_2-Agg and Gd_2O_3, but the cathepsin B inhibitor CA-074-Me (Figure 4D) and NLRP3 inflammasome inhibitor MCC950 (Figure S7) also had the same effect in KUP5 cells.

2.4. MoS_2 Induced Cellular Apoptosis through Mitochondrial ROS Production

Figures 1E and 1F show that MoS_2 nanosheets are capable of inducing ROS, reflecting surface redox activity. It is also possible that the release of Mo ions by extra- and intracellular MoS_2 dissolution may contribute to the generation of cellular oxidative stress, resembling the effect of ZnO nanoparticles.[22,53] Mitochondrial ROS production was assessed in KUP5, LSEC, and Hepa 1–6 cells by confocal microscopy, using MitoSOX red fluorescence intensity (Figure 5A). While MoS_2-Agg and MoS_2-PF could induce the dye oxidation in KUP5 cells, comparable to ZnO, there was no effect by aggregated or dispersed BN materials. Quantitative expression of the fluorescence intensity in a microplate reader confirmed that mtROS production in KUP5 cells, treated with MoS_2-Agg and MoS_2-PF, was significantly higher than treatment with similar BN materials (Figure 5B). Interestingly, MoS_2-PF induced a stronger response than MoS_2-Agg ($p < 0.05$).

Cellular oxidative stress is capable of inducing apoptosis, including through the perturbation of mitochondrial PT pores, capable of triggering caspase-induced cell death.[56] Confocal microscopy was used to assess the specific cleavage of a fluorescent FAM-FLICA caspase 3/7 substrate. The confocal images in Figure 6A demonstrate robust protease activation by MoS_2-Agg and MoS_2-PF in KUP5 but not LSECs or Hepa 1–6. Quantitative expression of the data, using a microplate reader, confirmed the confocal data (Figure 6B). The results demonstrated that MoS_2-PF mounted a significantly stronger response than MoS_2-Agg ($p < 0.05$). Flow cytometry analysis, looking at dual Annexin V-FITC/PI staining, also confirmed the appearance of 11.6% and 18.6% dual-positive KUP5 cells during exposure to MoS_2-Agg and MoS_2-PF, respectively (Figure S8). In contrast, BN-Agg and BN-PF did not show significant evidence of apoptosis. These data are in agreement with mitochondrial ROS production. Additionally, Mo (VI) also induced caspase 3/7 activation in KUP5 cells, similar to MoS_2-Agg and MoS_2-PF (Figure S9). This result confirms the notion that MoS_2 toxicity can be attributed to the release of soluble Mo (VI).

Figure 7 schematically summarizes the toxicity pathways that are engaged by MoS_2 in KUP5 cells. The extra- and intracellular dissolution of aggregated and dispersed MoS_2, release soluble Mo (VI) that is responsible for ROS generation, caspase 3/7 activation, and apoptotic cell death (Figure 7A and 7B). Moreover, the phagocytosis of MoS_2 induces lysosomal damage, cathepsin B release, caspase-1 activation, IL-1β and IL-18 secretion. (Figure 7A). Different from graphene oxide, fumed silica, and Gd_2O_3 nanoparticles,[36,56] MoS_2 did not generate pyroptosis in KUP5 cells as a result of the delayed activation of caspase-1, which could fail to generate the gasdermin D cleavage fragments that are required for the formation of the surface membrane pores.[56] The higher dissolution rate of MoS_2-PF and release of Mo (VI) is responsible for mitochondrial ROS production, caspase 3/7 activation, and apoptosis in KUP5 cells (Figure 7B).

3. Discussion

In this study, we assessed the effects of aggregated or Pluronic F87-dispersed BN and MoS_2 on three major liver cell types. Our results demonstrate a differential response of BN *vs.* MoS_2 materials, differences in the response of aggregated *vs.* dispersed MoS_2, and differences in the susceptibility of KUP5 *vs.* LSECs or Hepa 1–6 cells. While both MoS_2-Agg and MoS_2-PF triggered significant dissolution-dependent cytotoxicity in KCs, no significant toxicity was observed in LSECs and hepatocytes. In contrast, the BN materials did not induce toxicity in any of the cell types, irrespective of the dispersion status. Although Mo release from both MoS_2 materials contributed to ROS generation and led to caspase-induced apoptosis in KUP5 cells, the higher cytotoxicity of MoS_2-PF was independent of total cellular Mo content, which was the highest for MoS_2-Agg. This reflects phagocytic uptake of aggregated MoS_2, which triggers an additional response pathway that involves lysosomal damage, NLRP3 inflammasome activation, caspase-1 activation, IL-1β and IL-18 release. Since this response pathway is not triggered by MoS_2-PF or Mo (VI), the implication is that Mo release acts as an activator for the induction of apoptosis. This is compatible with the increased rate of cell death in response to the MoS_2-PF supernatant compared to the 2D pellet, which agrees with increased Mo (VI) on the MoS_2-PF surface compared to the aggregated material. This suggests that a higher rate of oxidative dissolution can explain MoS_2-PF toxicity. All considered, these data demonstrate important differences in the cytotoxic potential of two major classes of 2D nanomaterials that are increasingly being used for biological applications, with accompanying potential to come into contact with the liver.

An important finding of the current study is the delineation of the differential cytotoxic effects of BN and MoS_2 in KCs, LSECs, and hepatocytes. Although BN or MoS_2 are generally considered as biocompatible materials, some literature reports have suggested adverse cellular impacts, but without reference to specific liver cells. In contrast to MoS_2, BN nanosheets did not show significant toxicity in liver cells, which do not take up significant quantities of BN-Agg or BN-PF. In contrast, both MoS_2-Agg and MoS_2-PF induced significant cytotoxicity in KUP5 cells, with MoS_2-PF showing more robust effects that are duplicated by the supernatants rather than the pellets. Similar results could be generated by a soluble Mo (VI) salt.

How do we explain the enhanced susceptibility of KUP5 to the Mo released compared to the impact of the 2D nanosheet structure? In their study of the cytotoxic effects of MoS_2 on human hepatoma HepG2 cells, Liu *et al.* have shown that the MoS_2 leads to decreased cell viability through triggering of a cellular response pathway that involves cellular ROS generation, mitochondrial depolarization, as well as disruption of surface membrane function.[22] This includes inhibition of the transmembrane ATP-binding cassette (ABC) efflux transporter activity.[22] To differentiate between the membrane damaging activity of the MoS_2 sheetlike structure *vs.* the release of soluble Mo species, further experimentation was used to demonstrate that while soluble Mo does not induce oxidative stress or mitochondrial depolarization in HepG2 cells, Mo ions could interfere in ABC transporter activity.[22] This stands in contrast with our finding that the soluble MoS_2 fraction plays a key role in generating KUP5 toxicity, with the aggregated material pellet exerting

independent cellular effects. Several reports have shown that the dissolved 2D MoS_2 materials are capable of releasing MoO_4^{2-} in biological environments or environmental systems,[21,49,57] including the possibility to generate cellular toxicity under a variety of pH conditions.[49]

While the precise molecular basis for the toxicity of soluble Mo still needs to be clarified, it is well known that this transition element can be incorporated into the active center of a range of metalloenzymes.[58] This includes enzymes playing a role in ROS generation and redox cycling, such as aldehyde oxidase, xanthine oxidase, and hepatic sulfite oxidase.[58] We also know that high Mo concentrations can disrupt the active enzyme center and that molybdate ions can interact with divalent metal cations. For example, MoO_4^{2-} can bind to Cu^{2+} to form insoluble $CuMoO_4$, leading to copper depletion, interfering in Cu/Zn-SOD activity, and generating oxidative stress.[59,60] These mechanistic responses could form the basis of the enhanced MoS_2-PF toxicity, with material dispersion in Pluronic F87 facilitating oxidative dissolution of the nanosheets.[21,57] Here it is important to mention the importance of the dispersion protocol in avoiding toxicity generation by detergents or organic solvents, frequently used to increase 2D material dispersal. Our study was originally earmarked to assess with BN and MoS_2 nanosheets from a material source provided by NIEHS Nanotechnology Health Implications Research (NHIR) consortium, providing these materials as sodium cholate suspensions (Table S1). Although providing good 2D material dispersion, cholate is capable of inducing cytotoxic effects in a number of cell types.[49,61,62] Although some cell types may be less afflicted by cholate, we observed that all the liver cell types used in our study are adversely impacted by the above-threshold cholate concentrations present in the consortium suspensions (Figure S10). It should also be noted that strong binding of sodium cholate to nanomaterial services can also make toxicity assessment difficult, even if the excess cholate in the medium was removed. This precluded a meaningful assessment of the material adverse effects in liver cells. Instead, we used a non-toxic Pluronic polymer for 2D hazard assessment,[33] in addition to using Pluronic F87 to obtain dispersed and aggregated materials, a known physicochemical variation that determines 2D material hazard under biological conditions.[33,49, 63,64]

In addition to the biological impact of Mo (VI) release from MoS_2, we obtained evidence that phagocytic uptake of MoS_2-Agg can trigger lysosomal damage in KUP5 cells, leading to activation of the NRLP3 inflammasome and IL-1β and IL-18 production. Using various endocytosis inhibitors, we found that phagocytosis inhibition by wortmannin could significantly reduce the cellular uptake of MoS2-Agg. Moreover, the phagocytized MoS_2 could induce caspase-1 activation as well as IL-1β production, which was reduced by the introduction of inhibitors of the NRLP3 inflammasome, cathepsin B inhibitor, or the lysosomal proton pump. These findings are compatible with the notion that cathepsin B release from damaged lysosomes results in the activation of the NLRP3 inflammasome, as demonstrated for Gd_2O_3.[36] These results are in agreement with the demonstration by Yang *et al* that MoS_2 quantum dots can induce NRLP3 activation in the context of triggering a pyroptosis response in microglial cells.[65] It is also known that NRLP3 inflammasome activation can play an important role in hepatic inflammation and fibrosis during exposure to a number of injurious stimuli.[30,66]

It is worth mentioning that while KUP5 cells can respond to Gd_2O_3 or graphene oxide nanoparticles with pyroptosis,[36,67] a form of cell death, characterized by cell swelling and surface blebbing. The same effect was not observed with MoS_2-Agg in spite of caspase-1 activation. We suspect that the absence of pyroptosis during MoS_2-Agg exposure is due to early (~5 hr) activation of caspases 3/7 (Figure S9), which is responsible for gasdermin D cleavage at sites preventing the generation of caspase 1-induced pore-forming fragments.[68] These pore-forming subunits are responsible for the membrane permeabilization and giant surface membrane blebbing that characterizes the pyroptosis response. Our results are compatible with the recent demonstration that V_2O_5 nanoparticles induce caspase 3 and 7 activation, which interfere in the generation of gasdermin pore-forming subunits and pyroptosis in KUP5 cells.[56]

Why does MoS_2 fail to exert cytotoxic effects in hepatocytes and LSECs? While for MoS_2-Agg the obvious explanation is the phagocytic activity of KUP5 cells, the *in vivo* study by Cao *et al.* also showed the sequestration of protein-coated MoS_2@HSA nanocomplexes by Kupffer cells and the uptake of by Kupffer cells was around 5.4- to 9.2-fold higher than that by hepatocytes,[69] however, this does not explain the lack of cytotoxicity of dissolvable MoS_2-PF in these cells. Another explanation is the different sensitivity to nanomaterial toxicity among KCs, LSECs, and hepatocytes.[70] While this could be due to differences in membrane uptake of soluble Mo or the cellular defense against oxidative stress, elucidation of these mechanistic differences will require further study.

What lessons can be drawn from our results about the possible hepatotoxicity of a 2D nanomaterial such as MoS_2? In this study, we observed that the major impact of released Mo is on the KC cell line. The cross-communication between KCs and hepatocytes plays an important role in liver homeostasis.[30] KCs protect hepatocytes by removing cellular debris and particulate matter in what essentially amounts to a “janitorial” function, depending on phagocytosis, phagolysosome processing, and the release of degradation products. Also, the interactions between hepatocytes and KC involve an anti-inflammatory feedback loop that can be accomplished by decreased TNF-α release or increased IFN-β and IL-10 production.[71] KCs also regulate and maintain the detoxifying functions of hepatocytes, e.g., regulation of the expression of drug transporters (e.g., MRP3 and MRP4) or chemical transformation pathways mediated by cytochrome P450 enzymes.[30,66] However, despite these concerns there is currently no direct evidence for MoS_2-induced hepatotoxicity except the documentation of pro-inflammatory effects (e.g., IL-1β, IL-6, and AIF gene) and occurrence of apoptosis in the liver tissue of zebrafish.[27] Additional experimentation in rodents is required for the further assessment of MoS_2 safety *in vivo*.

4. Conclusions

In this study, we show differences in the toxicity of BN *vs.* MoS_2 nanosheets in KUP5 liver cells, without an impact on LSECs and Hepa 1–6 cells. While both MoS_2-Agg and MoS_2-PF induced significant cytotoxicity in KCs, the toxicity of the more dissolvable MoS_2-PF was higher and reflects increased release of Mo (VI) from the material surface. The soluble fraction was responsible for the generation of oxidative stress, activation of caspases 3/7, and apoptotic cell death. In addition, the phagocytosis of MoS_2-Agg triggered lysosomal

damage, cathepsin B release, NLRP3 inflammasome activation, and caspase-1 activation, leading to IL-1β and IL-18 production without evidence of pyroptosis. Overall this study provides a detailed mechanistic explanation for the differential toxicity of 2D BN- and MoS_2 nanosheets on liver cells.

5. Experimental Section

Materials:

The mouse Kupffer cell line, KUP5, was purchased from RIKEN Cell Bank (Japan). The immortalized mouse liver sinusoidal endothelial cells-SV40 (LSECs), Prigrow I medium (TM001), and flasks for growing LSECs were purchased from Applied Biological Materials (Vancouver, BC, Canada). The mouse hepatocyte cell line, Hepa 1−6, was purchased from ATCC. The CellTiter 96 aqueous one solution cell proliferation assay (MTS) and GSH-Glo glutathione assay kits were purchased from Promega (Madison, WI). Hoechst 33342 was purchased from Life Technologies (Grand Island, NY). MitoSOX indicator and 2′,7′-dichlorodihydrofluorescein diacetate (H_2DCFDA) were purchased from Invitrogen (Carlsbad, CA). The FAM-FLICA Caspase-1, Caspase-3/7, and Magic Red Cathepsin B assay kits were purchased from ImmunoChemistry Technologies, LLC (Bloomington, MN). The lipopolysaccharide (LPS), wortmannin (WM), cytochalasin D (Cyto D), nigericin, CA-074-Me, and MCC950 were purchased from Sigma (St. Louis, MO). The ELISA kits for mouse IL-1β and IL-18 were purchased from R&D Systems (Minneapolis, MN).

Preparation of Particle Suspensions:

The BN and MoS_2 dispersions were prepared as follows: The Pluronic F87 dispersions of BN and MoS_2 were prepared by immersing 300 mg of BN or MoS_2 powder in 8 mL of 2% w/v Pluronic F87 (BASF) solution in DI water, before ultrasonication for 1 h at a power of 16 W. The slurry was centrifuged to remove any non-exfoliated material and aggregates by retaining only the top 80% of the supernatant. The solution was concentrated by vacuum evaporation after a three-day dialysis procedure to remove excess Pluronic F87. The solutions were placed in 20 kDa molecular cut-off dialysis cassettes against DI water, and the DI water was replaced after the first 24 hours, resulting in the removal of excess Pluronic F87 in the solution. The aggregated BN and MoS_2 (BN-Agg and MoS_2-Agg) were prepared from the PF87 dispersions by inducing flocculation through the addition of four parts isopropyl alcohol to one part PF87 dispersion. The aggregates were filtered from the solution and rinsed thoroughly with DI water, and then resuspended by bath sonication in DI water. The flocculation step destabilizes the Pluronic F87 on the surface of the 2D material by introducing a competing solvent which increases the solubilization of the polymer. Subsequently, the 2D materials form large aggregates which are then easily filtered from the solution. The concentrations of the BN and MoS_2 solutions were measured by ICP-MS as described previously.[33] Briefly, BN and MoS_2 solutions were digested overnight at 65 °C in 70% nitric acid and subsequently diluted with water and internal standard. Using the ICP-MS measurements, concentration was inferred stoichiometrically.

Physicochemical Characterizations of BN and MoS_2:

The thickness and lateral size distributions of particles were assessed by AFM. Briefly, 300 nm SiO_2 on Si wafers functionalized with a monolayer of 2.5 mM (3-aminopropyl)-triethoxysilane (APTES) on the surface were rinsed with filtered DI water and dried under N_2. The samples were drop cast on the wafer and underwent heat treatment at 250 °C for 0.5 h. AFM images were obtained with the same tip and scanning conditions by an Asylum Research Cypher ES AFM. All images were taken at random locations on the sample and showed little variation. Since BN-Agg and MoS_2-Agg are beyond the size range for AFM measurements, SEM analysis was performed to characterize their particle size.

To investigate the chemical state and calculate the atomic concentration of functional groups on the BN and MoS_2 surface, a large amount of BN or MoS_2 was vacuum filtered onto anodized alumina membranes with a pore size of 0.1 μm and dried at room temperature. XPS analysis was performed using a Thermo Scientific ESCALAB 250Xi with a monochromatic Al Kα X-ray source at Northwestern University. The collected spectra were analyzed using a Smart background correction and peak fitting using Thermo Avantage software.

The stock solutions at a concentration of approximately 1 mg/mL in DI water were prepared and sonicated for 1 min to characterize the BN and MoS_2 in suspension. These suspensions were subsequently diluted to a final concentration of 50 μg/mL in DI water or cell culture media, followed by further sonication for 1 min. The hydrodynamic diameters, PDI, and zeta potentials of suspensions were determined using a ZetaPALS instrument (Brookhaven Instrument, Holtsville, NY).

Assessing the Intrinsic Oxidative Potential of BN and MoS_2:

Abiotic ROS generation by BN or MoS_2 was assessed using H_2DCFDA fluorescence. The DCF working solution was prepared by dissolving 50 μg H_2DCFDA in 17.3 μL ethanol, and 692 μL of a 0.01 mol/L sodium hydroxide solution was added. The resulting solution was incubated for 30 min, followed by adding 3500 μL of a sodium phosphate buffer (pH 7.4, 25 mmol/L) to form a 29 μmol/L DCF solution. Then, 80 μL of DCF was added to each well of a 96 multiwell black plate (Costar, Corning, NY). A 20 μL amount of 25 μg/mL BN or MoS_2 suspension was subsequently added to each well, followed by 2 h incubation. DCF fluorescence emission spectra in the range of 500–600 nm were collected using a SpectraMax M5e microplate reader with an excitation wavelength of 490 nm. The treatment of ZnO was used as a positive control.

The assessment of GSH content was obtained by using a GSH-Glo glutathione assay, a luminescence-based assay for detecting and quantifying glutathione (GSH) based on the conversion of a luciferin derivative to luciferin by glutathione S-transferase (GST). The assay was performed under abiotic conditions by adding 10 μL aliquots of BN and MoS_2 at 25 μg/mL to a 96-well white plate together with 90 μL of GSH-Glo agent for 30 min. The luciferin detection agent was added to each well (100 μL/well), and the luminescence was detected by a SpectraMax M5e microplate reader. The ZnO treatment was used as a positive control.

Cell Culture:

KUP5 cells were cultured in high-glucose Dulbecco's modified Eagle medium (DMEM), supplemented with 10% fetal bovine serum (Gemini Bio-Products, West Sacramento, CA), 100 U/mL to 100 μg/mL of penicillin-streptomycin (Gibco, Waltham, MA), 250 μM 1-thioglycerol, and 10 μg/mL bovine insulin. LSECs cells were cultured in the Prigrow medium, supplemented with 5% FBS and 100 U/mL to 100 μg/mL of penicillin-streptomycin. Hepa 1–6 cells were cultured in high-glucose DMEM medium, supplemented with 10% FBS and 100 U/mL to 100 μg/mL penicillin-streptomycin.

Determination of BN and MoS_2 Cytotoxicity:

The cell viability of KUP5, LSEC, and Hepa 1–6 cells was performed using the MTS assay. Cells seeded at a density of 4×10^4/well were exposed to the BN and MoS_2 particles at the indicated concentrations of 0–100 μg/mL for 24 h in 96-well plates (Corning, NY), respectively. The cell culture media were removed, followed by the replacement with 100 microliters of complete culture media containing 16.7% MTS stock solution for 0.5 h in a humidified 5% CO_2 incubator. The plates were centrifuged at 2000 rpm for 10 min in an Eppendorf 5430 microcentrifuge to spin down the cell debris and particles, and then an 80 μL amount of the supernatant was collected from each well and transferred into a new 96-well plate. The absorbance of formed formazan was read at 490 nm on a SpectraMax M5e microplate reader (Molecular Devices, Sunnyvale, CA). Non-treated or control cells (0 μg/mL) were considered to exhibit 100% cell viability, according to which the viability of the treated cells was adjusted. ZnO nanoparticles were used as a positive control.

Determination of Particle Dissolution in DI Water and Culture Medium:

Following suspension in DI water and DMEM medium for 24 h at 37 °C, the pellets of BN and MoS_2 were collected by centrifugation at 15 000 rpm for 50 min. The supernatants were removed and subjected to acid digestion, using a 10 mL mixture of concentrated HNO_3 (65−70%, trace metal grade, Fisher Scientific) and HCl (35−38%, trace metal grade, Fisher Scientific) in a ratio of 1:3 at 95 °C for 2 days in a HotBlock (SC100, Environmental Express). The B or Mo content was determined by ICP-MS (NexION 2000, PerkinElmer, Waltham, MA), using triplicate analysis of each sample and standard in the presence of 2% (v/v) nitric acid. The digested cell culture media and DI water without particles were served as a blank reagent.

Assessment of Cellular Uptake of BN and MoS_2:

KUP5, LSEC, and Hepa 1–6 cells were exposed to 25 μg/mL BN and MoS_2 for 16 h. The cell morphological change by BN or MoS_2 was monitored using a Zeiss Optical Microscope (Carl Zeiss Inc., Peabody, MA). To quantify the cellular uptake of particles at 25 μg/mL, following an incubation period of 16 h, the cellular pellets were collected and treated in lysis buffer for 30 min at 4 °C. The pellets were collected by centrifugation at 15 000 rpm for 30 min and digested by concentrated nitric acid at 90 °C for 3 h. The digested solutions were dried by evaporation at 120 °C and dissolved in 3 mL of 5% nitric acid to assess B or Mo content by ICP-MS.

Determination of mtROS Generation by BN and MoS_2:

KUP5, LSEC, and Hepa 1–6 cells, exposed to BN and MoS_2 for 16 h, were washed with PBS and treated with 5 μM MitoSOX in HBSS at 37 °C for 10 min. The cells were stained with 5 μg/mL Hoechst 33342 for 15 min, fixed with 4 % paraformaldehyde in PBS, and imaged by a Leica Confocal SP8-SMD microscope (Leica, Germany). The quantification for fluorescence intensity was monitored as the rate of oxidation of the dye in the cells at excitation/emission wavelengths of 510/580 nm by a microplate reader. The treatment of ZnO was used as a positive control.

Determination of the activation of Caspases 3/7:

KUP5, LSEC, and Hepa 1–6 cells, seeded at 2×10^5 cells/well in an 8-well Lab-Tek chamber slide, were incubated with 25 μg/mL of BN and MoS_2, respectively. The treated cells were washed in PBS and stained with FAM-FLICA Caspases 3/7 substrates at 37 °C for 1 h according to the manufacturer's instructions. Finally, the cells were stained with Hoechst 33342 for 15 min and imaged using a Leica Confocal SP8-SMD microscope. The quantification for fluorescence intensity in the cells was monitored at excitation/emission wavelengths of 492/520 nm by a microplate reader. ZnO nanoparticles were used as a positive control.

Determination of Apoptosis via Annexin-V Staining and Flow Cytometry:

KUP5 cells were plated at a density of 5×10^5 cells per well in a 6-well plate overnight. The medium was replaced with a fresh medium in the presence of LPS (1 μg/mL) and incubated for an additional 4 h. The primed KUP5 cells were treated with 25 μg/mL particles for 16 h, respectively. After the collection of the cell pellets, followed by washing in PBS, the Annexin V-FITC Apoptosis Detection Kit was used for cellular staining according to the manufacturer's procedure. The cells were analyzed with a BD LSR II Flow Cytometer by using FITC and PE channels for the detection of Annexin V-FITC and PI staining, respectively. Finally, the flow cytometry results were analyzed with FCS Express 6 software to identify Annexin V/PI-positive cells as apoptotic populations and Annexin V-negative/PI-positive cells as populations undergoing nonapoptotic cell death.

Determination of Caspase-1 Activation in KUP5 Cells:

The KUP5 cells, primed with LPS (1 μg/mL) for 4 h, were incubated with 25 μg/mL particles, followed by washing in PBS and staining with FAM-FLICA caspase-1 substrate for 1 h at 37 °C. The cells were stained with Hoechst 33342 for 15 min and imaged using a Leica Confocal SP8-SMD microscope. The quantification for fluorescence intensity in the cells was monitored at excitation/emission wavelengths of 492/520 nm by a microplate reader. Treatment with Gd_2O_3 nanoparticles was used as a positive control that induces lysosomal damage.[36]

Determination of IL-1β and IL-18 Production:

KUP5 cells were primed by replacing the tissue culture medium with a fresh medium containing 1 μg/mL LPS for 4 h, followed by the exposure to 25 μg/mL of particle suspensions containing 0.1 μg/mL LPS for 24 h. The cellular supernatants were collected for

IL-1β or IL-18 quantification by ELISA according to the manufacturer's instructions. The treatment of Gd_2O_3 was used as a positive control.[36]

Statistical Analysis:

All statistical analysis was performed, using a two-tailed Student's t-test for two-group analysis or one-way ANOVA for multiple group comparisons. The results were expressed as the mean plus and minus standard deviation, using three independent experiments. A *p*-value of less than 0.05 was considered statistically significant.

Supplementary Material

Refer to Web version on PubMed Central for supplementary material.

Acknowledgments

The research reported in this publication was supported by the Nanotechnology Health Implications Research (NHIR) Consortium of the National Institute of Environmental Health Sciences of the National Institutes of Health under Award Number (U01ES027237). The content is solely the responsibility of the authors and does not necessarily represent the official views of the National Institutes of Health. Cholate-suspended BN and MoS_2 nanosheets were procured/developed, characterized, and provided by the Engineered Nanomaterials Resource and Coordination Core established at T. H. Chan School of Public Health (NIH grant # U24ES026946) as a service core for the Nanotechnology Health Implications Research Consortium. The authors thank the CNSI Advanced Light Microscopy/Spectroscopy and Electron Imaging Center for NanoMachines Core Facilities and the Flow Cytometry Core Facility of Jonsson Comprehensive Cancer Center at UCLA. This work made use of the Keck-II facility of Northwestern University's NUANCE Center, which has received support from the SHyNE Resource (NSF ECCS-1542205), the IIN, and the Northwestern University MRSEC program (NSF DMR-1720139).

References

[1]. Chhowalla M, Shin HS, Eda G, Li LJ, Loh KP, Zhang H, Nat. Chem 2013, 5, 263. [PubMed: 23511414]

[2]. Hua Z, Hui-Ming C, Peide Y, Chem. Soc. Rev 2018, 47, 10.

[3]. Wang H, Yu L, Lee YH, Shi Y, Hsu A, Nano Lett. 2012, 12, 4674. [PubMed: 22862813]

[4]. Wu C, Zhang J, Tong X, Yu P, Chueh YU, Small 2019, 15, e1900578. [PubMed: 31165564]

[5]. Zhou W, Zou X, Najmaei S, Liu Z, Shi Y, Kong J, Lou J, Ajayan PM, Yakobson BI, Idrobo JC, Nano Lett. 2013, 13, 2615. [PubMed: 23659662]

[6]. Lembke D, Bertolazzi S, Kis A, Acc Chem Res 2015, 48, 100. [PubMed: 25555202]

[7]. Beck ME, Hersam MC, ACS Nano 2020, 14, 6498. [PubMed: 32463222]

[8]. Zhang X, Nie J, Yang X, Liu Z, Guo W, Qiu J, Wang S, Yu X, Guan Y, Liu H, Applied Materials Today 2017, S1281234527.

[9]. Liu Y, Peng J, Wang S, Xu M, Gao M, Xia T, Weng J, Xu A, Liu S, NPG Asia Mater. 2018, 10, e458.

[10]. Yadav V, Roy S, Singh P, Khan Z, Jaiswal A, Small 2019, 15, e1803706. [PubMed: 30565842]

[11]. Liu T, Wang C, Gu X, Gong H, Liu Z, Adv. Mater 2014, 26, 1886. [PubMed: 24375758]

[12]. Sabari Arul N, Nithya VD, RSC Adv. 2016, 6, 65670.

[13]. Luo W, Wang Y, Hitz E, Lin Y, Yang B, Hu L, Adv. Funct. Mater 2017, 27, 1701450.

[14]. Watanabe K, Taniguchi T, Kanda H, Nat. Mater 2004, 3, 404. [PubMed: 15156198]

[15]. Song L, Ci L, Lu H, Sorokin PB, Jin C, Ni J, Kvashnin AG, Kvashnin DG, Lou J, Yakobson BI, Nano Lett. 2010, 10, 3209. [PubMed: 20698639]

[16]. Loeblein M, Tsang SH, Pawlik M, Phua EJR, Yong H, Zhang XW, Gan CL, Teo EHT, ACS Nano 2017, 11, 2033. [PubMed: 28157329]

[17]. Kuang Z, Chen Y, Lu Y, Liu L, Hu S, Wen S, Mao Y, Zhang L, Small 2015, 11, 1655. [PubMed: 25365940]

[18]. Guiney LM, Mansukhani ND, Jakus AE, Wallace SG, Shah RN, Hersam MC, Nano Lett. 2018, 18, 3488. [PubMed: 29709193]

[19]. Nagarajan S, Belaid H, Pochat-Bohatier C, Teyssier C, Iatsunskyi I, Coy E, Balme S, Cornu D, Miele P, Kalkura NS, ACS Appl. Mater. Inter 2017, 9, 33695.

[20]. Ciofani G, Danti S, Genchi GG, Mazzolai B, Mattoli V, Small 2013, 9, 1672. [PubMed: 23423826]

[21]. Guiney LM, Xiang W, Tian X, Nel AE, Hersam MC, ACS Nano 2018, 12, 6360. [PubMed: 29889491]

[22]. Liu S, Shen Z, Wu B, Yu Y, Hou H, Zhang XX, Ren HQ, Environ. Sci. Technol 2017, 51, 10834. [PubMed: 28841301]

[23]. Li X, Wang X, Zhang J, Hanagata N, Wang X, Weng Q, Ito A, Bando Y, Golberg D, Nat. Commun 2017, 8, 13936. [PubMed: 28059072]

[24]. Zhang YN, Poon W, Tavares AJ, Mcgilvray ID, Chan WCW, Control J. Release 2016, 240, 332.

[25]. Shim G, Ko S, Park JY, Suh JH, Oh YK, Control J. Release 2020, 327, 616.

[26]. Wang S, Li K, Chen Y, Chen H, Shi J, Biomaterials 2015, 39, 206. [PubMed: 25468372]

[27]. Yu Y, Yi Y, Li Y, Peng T, Lao S, Zhang J, Liang S, Xiong Y, Shao S, Wu N, RSC Adv. 2018, 8, 17826.

[28]. Dixon LJ, Barnes M, Tang H, Pritchard MT, Nagy LE, Compr. Physiol 2013, 3, 785. [PubMed: 23720329]

[29]. David A, Hume, Curr. Opin. Immunol 2006, 1, 49.

[30]. Bilzer M, Roggel F, Gerbes AL, Liver Int. 2006, 26, 1175. [PubMed: 17105582]

[31]. Boey A, Ho HK, Small 2020, 16, e2000153. [PubMed: 32163668]

[32]. Tsoi KM, Macparland SA, Ma XZ, Spetzler VN, Echeverri J, Ouyang B, Fadel SM, Sykes EA, Goldaracena N, Kaths JM, Nat. Mater 2016, 15, 1212. [PubMed: 27525571]

[33]. Wang X, Mansukhani ND, Guiney LM, Ji Z, Chang CH, Wang M, Liao YP, Song TB, Sun B, Li R, Small 2015, 11, 5079 [PubMed: 26237579]

[34]. Horváth L, Magrez A, Golberg D, Zhi C, Schwaller B, ACS Nano 2011, 5, 3800. [PubMed: 21495683]

[35]. Lin H, Ji DU, Lucherelli MA, Reina G, Bianco A, Small 2020, 16, 2002194.

[36]. Mirshafiee V, Sun B, Chang CH, Liao Y, Jiang W, Jiang J, Liu X, Wang X, Xia T, Nel AE, ACS Nano 2018, 12, 3836. [PubMed: 29543433]

[37]. Sørensen KK, Simonsantamaria J, Mccuskey RS, Smedsrød B, Compr. Physiol 2015, 5, 1751. [PubMed: 26426467]

[38]. Kjeken R, Mousavi SA, Brech A, Gjoen T, Berg T, Cell Tissue Res. 2001, 304, 221. [PubMed: 11396716]

[39]. Poisson J, Lemoinne S, Boulanger C, Durand FO, Moreau R, Valla D, Rautou PE, J. Hepatol 2016, 212. [PubMed: 27423426]

[40]. Gissen P, Arias IM, J. Hepatol 2015, 63, 1023. [PubMed: 26116792]

[41]. Ciofani G, Turco SD, Genchi GG, Alessandro DD, Basta G, Mattoli V, Int. J. Pharmaceut 2012, 436, 444.

[42]. Ke SK, Lai Y, Zhou T, Li L, Wang Y, Ren L, Ye S, ACS Biomater. Sci. Eng 2018, 4, 663. [PubMed: 33418754]

[43]. Liu Q, Wang X, Liu X, Kumar S, Gochman G, Ji Y, Liao Y, Chang CH, Situ W, Lu J, Jiang J, Mei K, Meng H, Xia T, Nel AE, ACS Nano 2019, 13, 4778. [PubMed: 30964276]

[44]. Li H, Tay RY, Tsang SH, Zhen X, Teo EHT, Small 2016, 11, 6491.

[45]. Sobańska Z, Domeradzka-Gajda K, Szparaga M, Grobelny J, Stpnik M, Toxicol. in Vitro 2020, 68, 104931. [PubMed: 32640262]

[46]. Liu Q, Chen C, Du M, Wu Y, Ren C, Ding K, Song M, Huang C, ACS Applied Nano Materials 2018, 1, 4566.

[47]. Kondekar NP, Boebinger MG, Woods EV, Mcdowell MT, ACS Appl. Mater. Inter 2017, 9, 32394.

[48]. Woanseo Park, Jaeyoon Baik, Tae-Young Kim, Kyungjune Cho, Woong-Ki Hong,Nano ACS 2014, 8, 4961.

[49]. Wang Z, von Dem Bussche A, Qiu Y, Valentin TM, Gion K, Kane AB, Hurt RH, Environ. Sci. Technol 2016, 50, 7208. [PubMed: 27267956]

[50]. Zhang H, Pokhrel S, Ji Z, Meng H, Wang X, Lin S, Chang CH, Li L, Li R, Sun B, Wang M, Liao YP, Liu R, Xia T, Madler L, Nel AE, J. Am. Chem. Soc 2014, 136, 6406. [PubMed: 24673286]

[51]. Lundqvist M, Stigler J, Elia G, Lynch I, Cedervall T, Dawson KA, Proc. Natl. Acad. Sci. U S A 2008, 105, 14265. [PubMed: 18809927]

[52]. Wang C, Liang C, Yeh H, Chemosphere 2016, 147, 82. [PubMed: 26761601]

[53]. Tian X, Michael K, Monty L, Lutz M, Benjamin G, Haibin S, Joanne I Y, Jeffrey I Z, Andre E N, ACS Nano 2008, 2, 2121. [PubMed: 19206459]

[54]. Linares J, Matesanz MC, Vila M, Feito MJ, Gonçalves G, Vallet-Regí M, Marques PAAP, Portolés MT, ACS Appl. Mater. Inter 2014, 6, 13697.

[55]. Mauvezin C, Neufeld TP, Autophagy 2015, 11, 1437. [PubMed: 26156798]

[56]. Wang X, Chang CH, Jiang J, Liu X, Li J, Liu Q, Liao YP, Li L, Nel AE, Xia T, Small 2020, 16, e2000528. [PubMed: 32337854]

[57]. Lee T, Chen C, Chen C, Environ. Sci. Technol 2019, 53, 6282. [PubMed: 31062596]

[58]. Mendel RR, Bittner F, Biochim Biophys Acta 2006, 1763, 621. [PubMed: 16784786]

[59]. Torres J, Gonzatto L, Peinado G, Kremer C, Kremer E, Solution Chem J. 2014, 43, 1687.

[60]. Weidner E, Ciesielczyk F, Materials 2019, 12, 927.

[61]. Pattammattel A, Pande P, Kuttappan D, Puglia M, Basu AK, Amalaradjou MA, Kumar CV, Langmuir 2017, 33, 14184. [PubMed: 29144756]

[62]. Gao J, Llaneza V, Youn S, Silvera-Batista CA, Ziegler KJ, Bonzongo JJ, Environ. Toxicol. Chem 2012, 31, 210. [PubMed: 22002585]

[63]. Khattak SF, Bhatia SR, Roberts SC, Tissue Eng. 2005, 11, 974. [PubMed: 15998236]

[64]. Roy P, Das S, Auddy RG, Saha A, Mukherjee A, Pharm. Res 2013, 30, 1252. [PubMed: 23319171]

[65]. Yang P, Ke S, Tu L, Wang Y, Ye S, Kou S, Ren L, ACS Biomater. Sci. Eng 2020, 6, 1764.

[66]. Szabo G, Petrasek J, Nat. Rev. Gastro. Hepat 2015, 12, 387.

[67]. Li J, Wang X, Mei KC, Chang CH, Jiang J, Liu X, Liu Q, Guiney LM, Hersam MC,Liao YP, H Meng, Xia T, Nano Today 2021, 37, 101061. [PubMed: 34055032]

[68]. Taabazuing CY, Okondo MC, Bachovchin DA, Cell Chem. Biol 2017, 24, 507. [PubMed: 28392147]

[69]. Cao M, Cai R, Zhao L, Guo M, Wang L, Wang Y, Zhang L, Wang X, Yao H, Xie C, Cong Y, Guan Y, Tao X, Wang Y, Xu S, Liu Y, Zhao Y, Chen C, Nat. Nanotechnol 2021, 10.1038/s41565-021-00856-w.

[70]. Wang H, Thorling CA, Liang X, Bridle KR, Grice JE, Zhu Y, Crawford DHG, Xu ZP, Liu X, Roberts MS, J. Mater. Chem. B 2015, 3, 939. [PubMed: 32261972]

[71]. Knolle PA, Gerken G, Immunol. Rev 2000, 174, 21. [PubMed: 10807504]

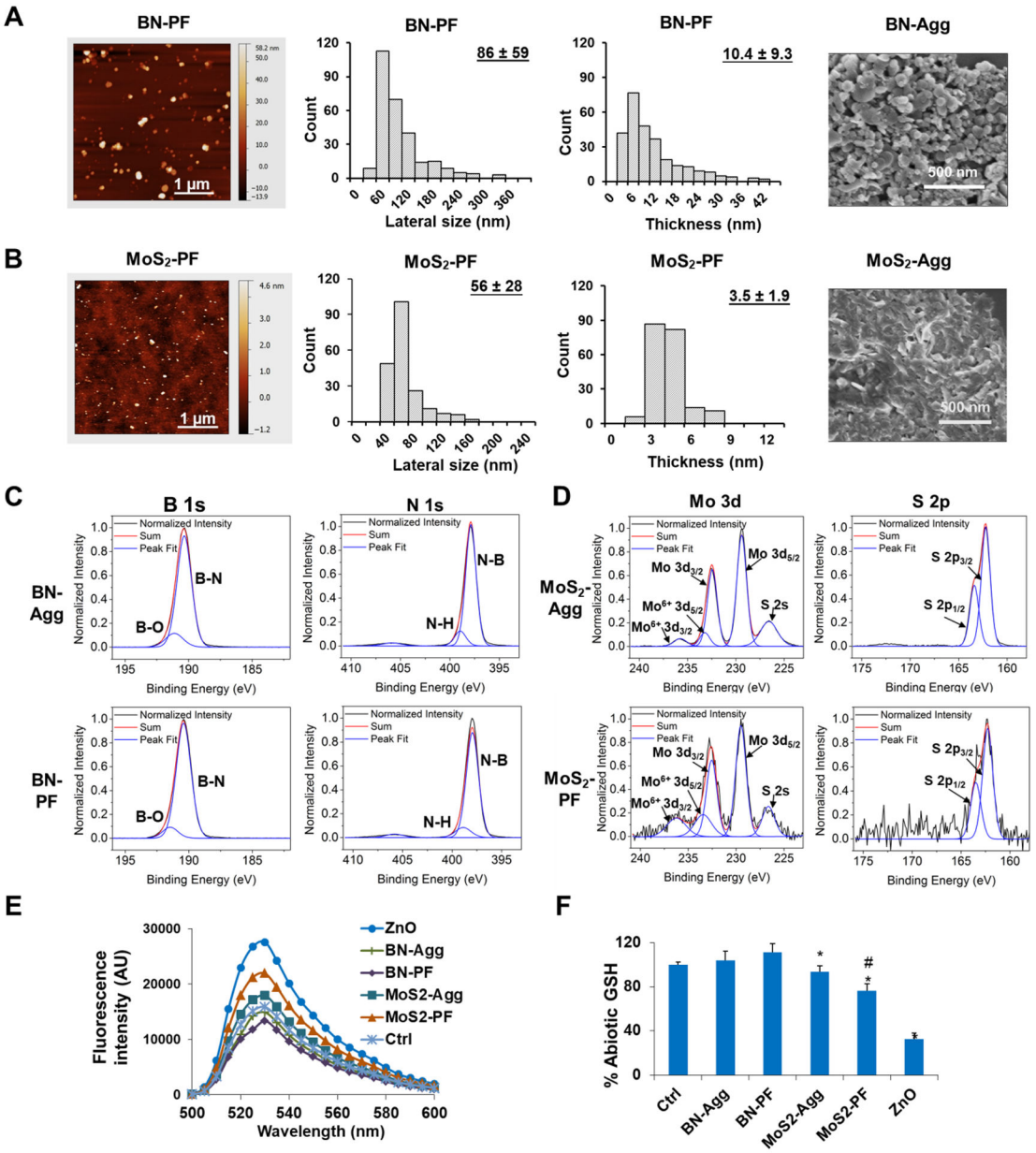

Figure 1. Physicochemical characterization of materials in the BN and MoS_2 library.

(A) Physicochemical characterizations of BN samples. The first panel is a representative AFM image of BN-PF, showing well-dispersed individual flakes; the second panel shows the lateral size distribution of BN-PF (the average lateral size is 86 ± 59 nm); the third panel shows the thickness distribution of BN-PF (the average thickness is 10.4 ± 9.3 nm); and the fourth panel is a representative SEM image of BN-Agg showing the aggregated state of the BN flakes as large agglomerates. (B) Physicochemical characterizations of MoS_2 samples. The first panel is a representative AFM image of MoS_2-PF, showing well-dispersed individual flakes of MoS_2; the second panel shows the lateral size distribution of MoS_2-PF (the average lateral size is 56 ± 28 nm); the third panel shows the thickness distribution, for which the average thickness is 3.5 ± 1.9 nm; and the fourth panel is a representative SEM

image of MoS_2-Agg showing the aggregated state of the MoS_2 flakes into large agglomerates. (C) Characterization of BN composition by XPS. The left panels show the B 1s core-level spectra of BN-Agg (upper row) and BN-PF (lower row); The panels on the right show the N 1s core-level spectra of BN-Agg (upper row) and BN-PF (lower row). (D) Characterization of MoS_2 composition by XPS. The left panels show the Mo 3d core-level spectra of MoS_2-Agg (upper row) and MoS_2-PF (lower row); The panels on the right show the S 2p core-level spectra of MoS_2-Agg (upper row) and MoS_2-PF (lower row). (E) H_2DCFDA fluorescence spectroscopy to show abiotic ROS generation by 25 μg/mL BN or MoS_2. DCF fluorescence emission spectra in the range of 500–600 nm were collected with an excitation wavelength of 490 nm. ZnO nanoparticles served as a positive control. (F) Assessment of the abiotic GSH content through the use of the GSH-Glo agent. The luminescence was detected in a SpectraMax M5e microplate reader, following the addition of 10 μL BN or MoS_2 at 25 μg/mL to 90 μL of the GSH-Glo agent. The asterisk (*) represents a p-value < 0.05, compared to the control,; # represents a p-value of < 0.05 in the comparison of MoS_2-Agg with MoS_2-PF.

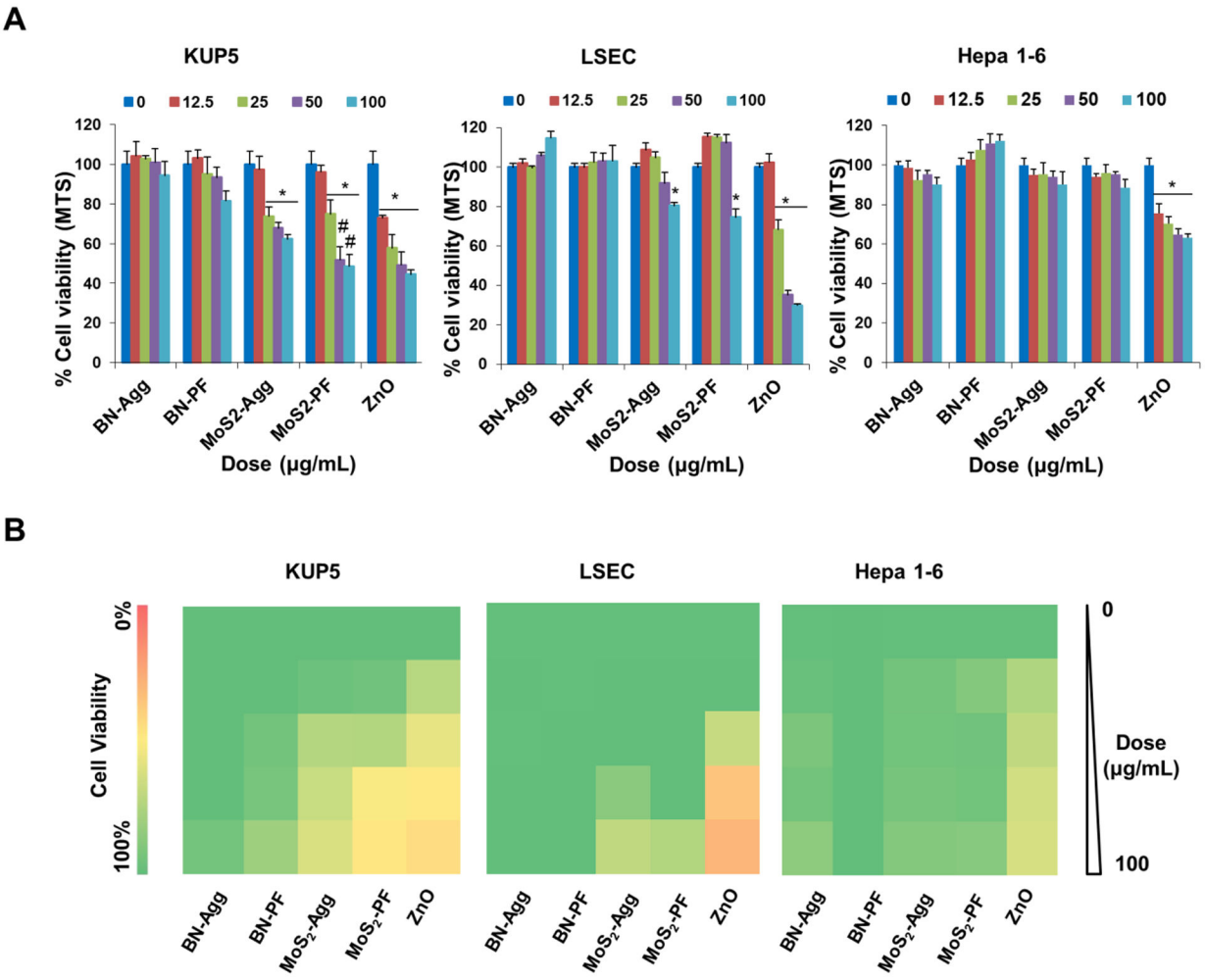

Figure 2. Use of an MTS assay to assess the viability of KUP5, LSEC, and Hepa 1–6 cells in response to the 2D nanosheets.

(A) Cell viability of KUP5, LSEC, and Hepa 1–6 cells after exposure to BN and MoS_2 at 0−100 μg/mL for 24 h. The viability of untreated cells was regarded as 100%. Treatment with ZnO nanoparticles was used as a positive control. The asterisk (*) represents a *p*-value < 0.05 compared to untreated cells, while # represents a *p*-value of < 0.05 for the comparison of MoS_2-Agg with MoS_2-PF. (B) Heatmap display to show the comparative toxicological impact on KUP5, LSEC, and Hepa 1−6 cells following the color scale in the sidebar on the left.

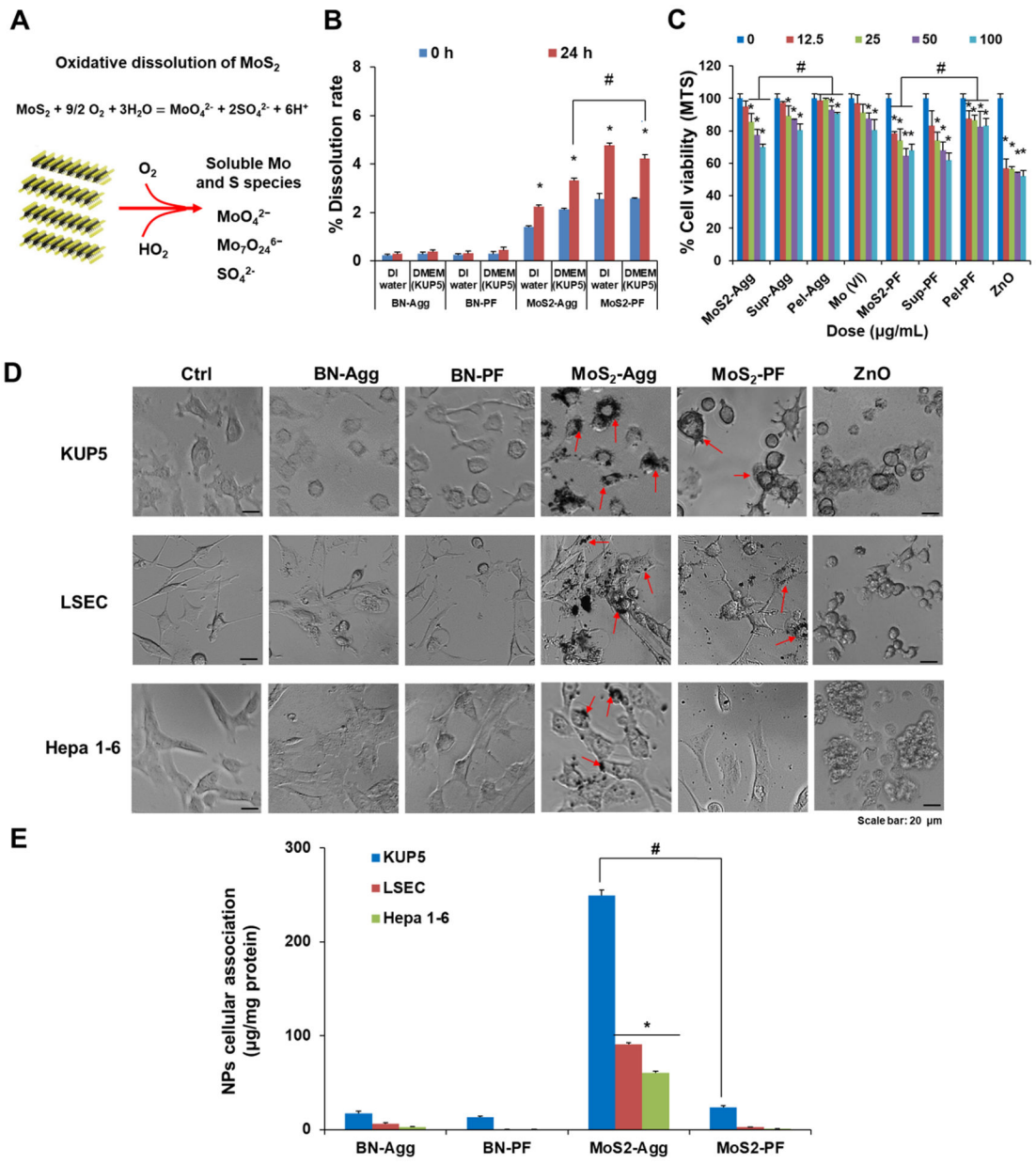

Figure 3. Assessment of the impact of material dissolution and uptake on KUP5 cytotoxicity.

(A) ICP-MS analysis to determine the dissolution of the BN and MoS_2 materials in DI water and DMEM medium. The materials were suspended at 25 μg/mL for 0 h and 24 h at 37°C before collection of the supernatants. The supernatants were subjected to acid digestion to assess the B or Mo content by a NexION 2000 ICP Mass Spectrometer. Each sample was analyzed in triplicate, in comparison to a reference standard made up of 2% (v/v) nitric acid. *, $p < 0.05$ to show significant differences between 0 h and 24 h; #, $p < 0.05$ to show the significant difference between MoS_2-Agg and MoS_2-PF treatments. (B) Assessment of the toxicity of starting MoS_2 suspensions, supernatants, and pellets, along with a soluble molybdate salt [Na_2MoO_4, Mo (VI)] in KUP5 cells. ZnO treatment was used as a positive control. *, $p < 0.05$, indicates a significant difference compared to the control; #, $p < 0.05$,

donates a significant difference between the MoS_2 suspensions and their pellets. (C) Optical microscopy images to show the relative abundance of nanosheet uptake by KUP5, LSEC, and Hepa 1–6 cells, exposed to 25 μg/mL of BN or MoS_2 for 16 h (red arrows). The scale bar in the image represents 20 μm. (D) Quantification of cellular uptake of BN or MoS_2 in KUP5, LSEC, and Hepa 1–6 cells during ICP-MS analysis. Following exposure to 25 μg/mL of the nanosheets for 16 h, cell pellets were acid digested and assessed B and Mo content, respectively. *, $p < 0.05$, to express the significant difference of KUP5 with LSECs or Hepa 1–6 cells; #, $p < 0.05$, to show the significant difference between MoS_2-Agg and MoS_2-PF.

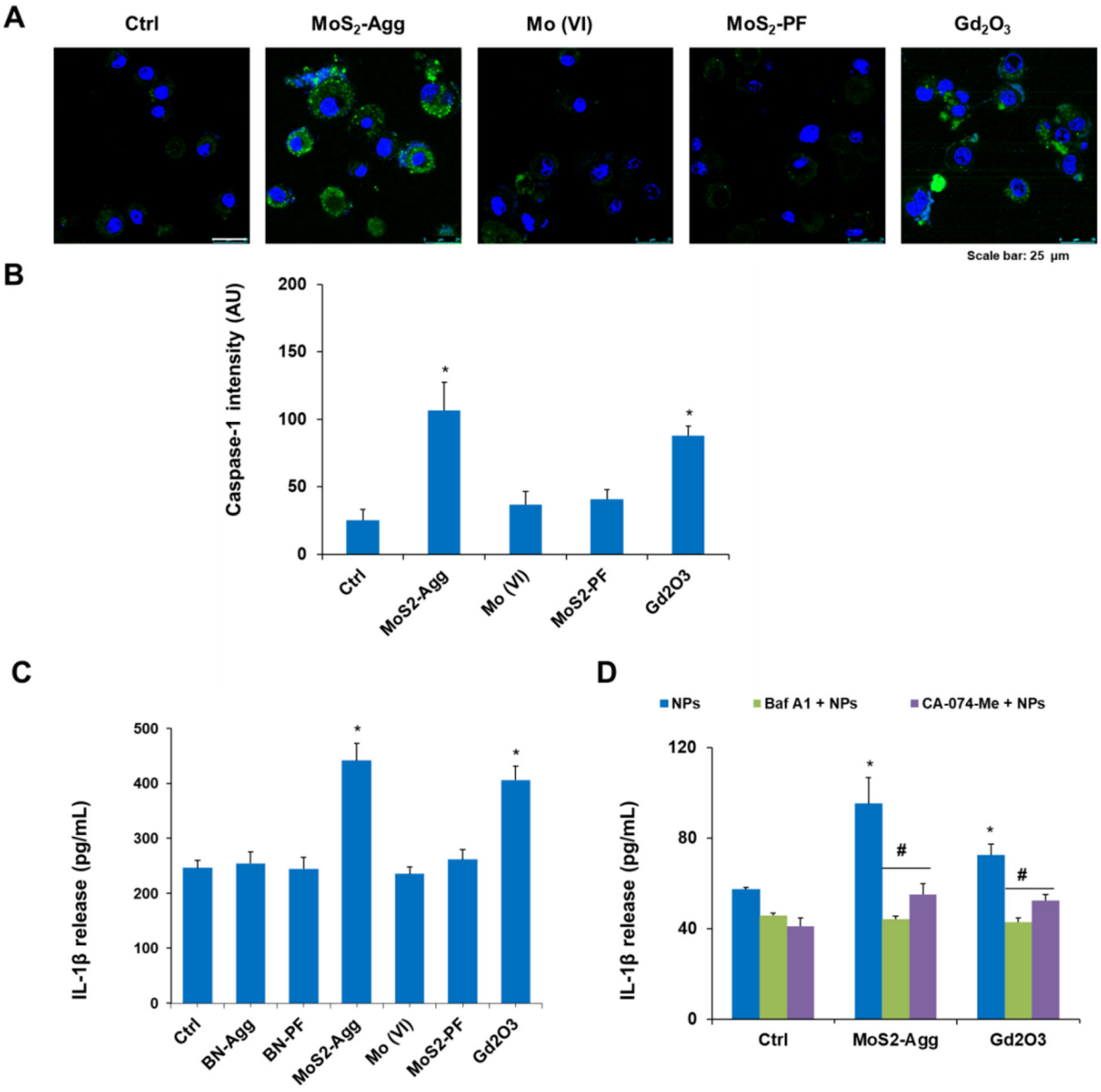

Figure 4. Use of confocal microscopy and ELISA to assess caspase-1 activation and IL-1β release in KUP5 cells, following phagocytic uptake of MoS_2.

(A) Confocal images to compare the differences in caspase-1 activation by MoS_2-Agg, Mo (VI), and MoS_2-PF in KUP5. Cells were exposed to 25 μg/mL of the materials for 16 h before staining with the FAM-FLICA caspase-1 substrate (green) for 1 h. Exposure to Gd_2O_3 nanoparticles, which disrupt lysosomal integrity, was used as a positive control. The scale bar in the image represents 25 μm. (B) Quantification of caspase-1 activation in cells treated with MoS_2 and Mo (VI) in a microplate reader. *, $p < 0.05$ to show the significant difference compared to the untreated control. (C) Determination of IL-1β release in KUP5 cells after BN, Mo (VI), and MoS_2 exposure. LPS-primed (1 μg/mL, 4 h) KUP5 cells were exposed to BN, Mo (VI), and MoS_2 for 24 h. Supernatants were collected to measure IL-1β production by ELISA. (D) Determination of IL-1β production by MoS_2-Agg in KUP5 cells

pretreated with V-ATPases inhibitor, Baf A1, and the cathepsin B inhibitor, CA-074-Me. The Gd_2O_3 treatment was used as a positive control. *, $p < 0.05$, shows a significant difference from the control; #, $p < 0.05$ shows a significant difference compared to treatment with the NP alone.

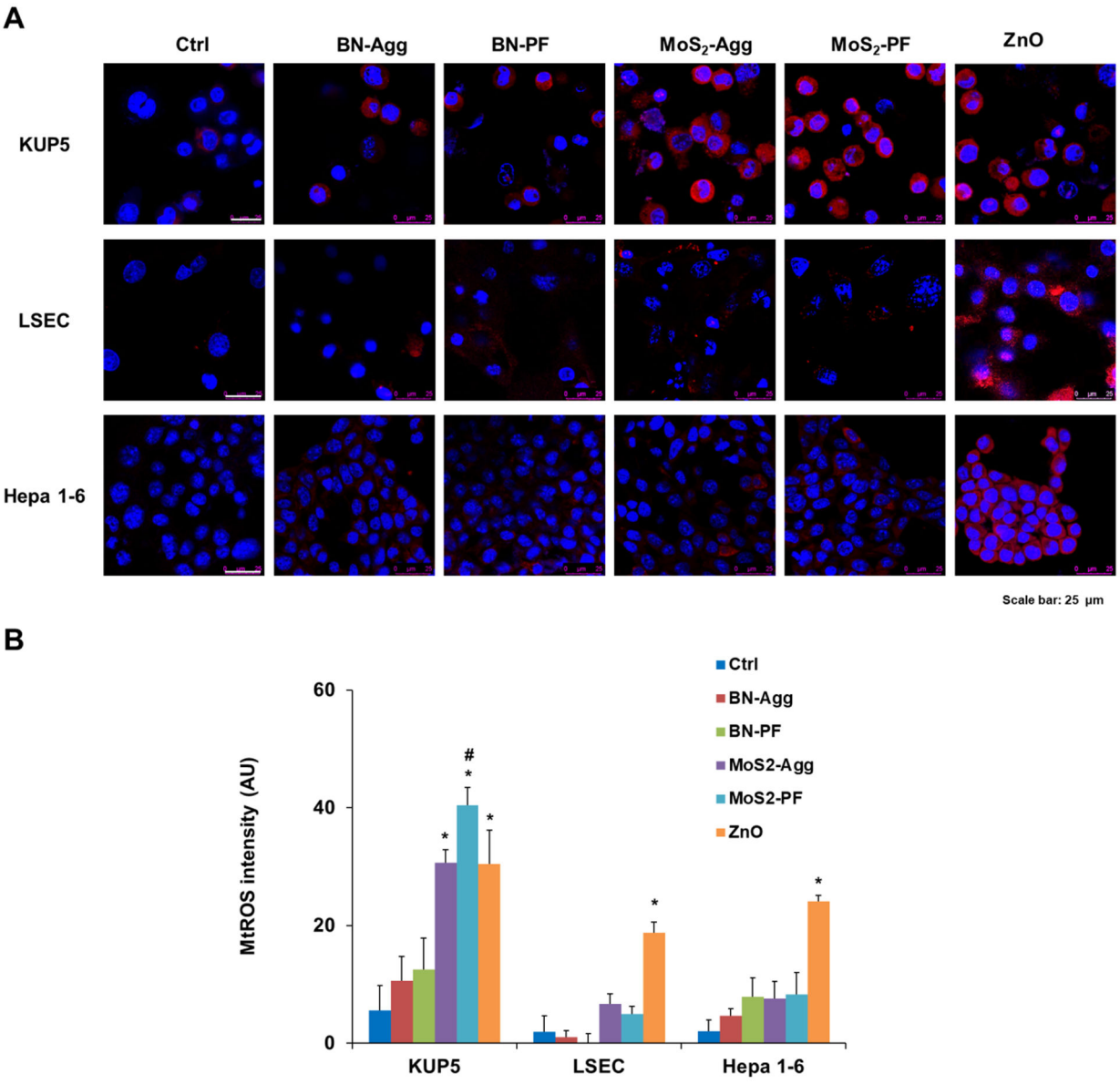

Figure 5. Assessment of mtROS generation in the liver cells.

(A) Confocal images to determine mtROS generation in KUP5, LSEC, and Hepa 1–6 cells. Cells were exposed to 25 μg/mL materials for 16 h before staining with 5 μM red MitoSOX for 10 min and Hoechst 33342 dye (blue) for 15 min, respectively. The scale bar represents 25 μm. (B) Quantification of mtROS generation, using a microplate reader. The fluorescence intensity was monitored at excitation/emission wavelengths of 510/580 nm. *, $p < 0.05$ shows the significant difference compared to the untreated control; #, $p < 0.05$ denotes a significant difference between MoS_2-Agg and MoS_2-PF.

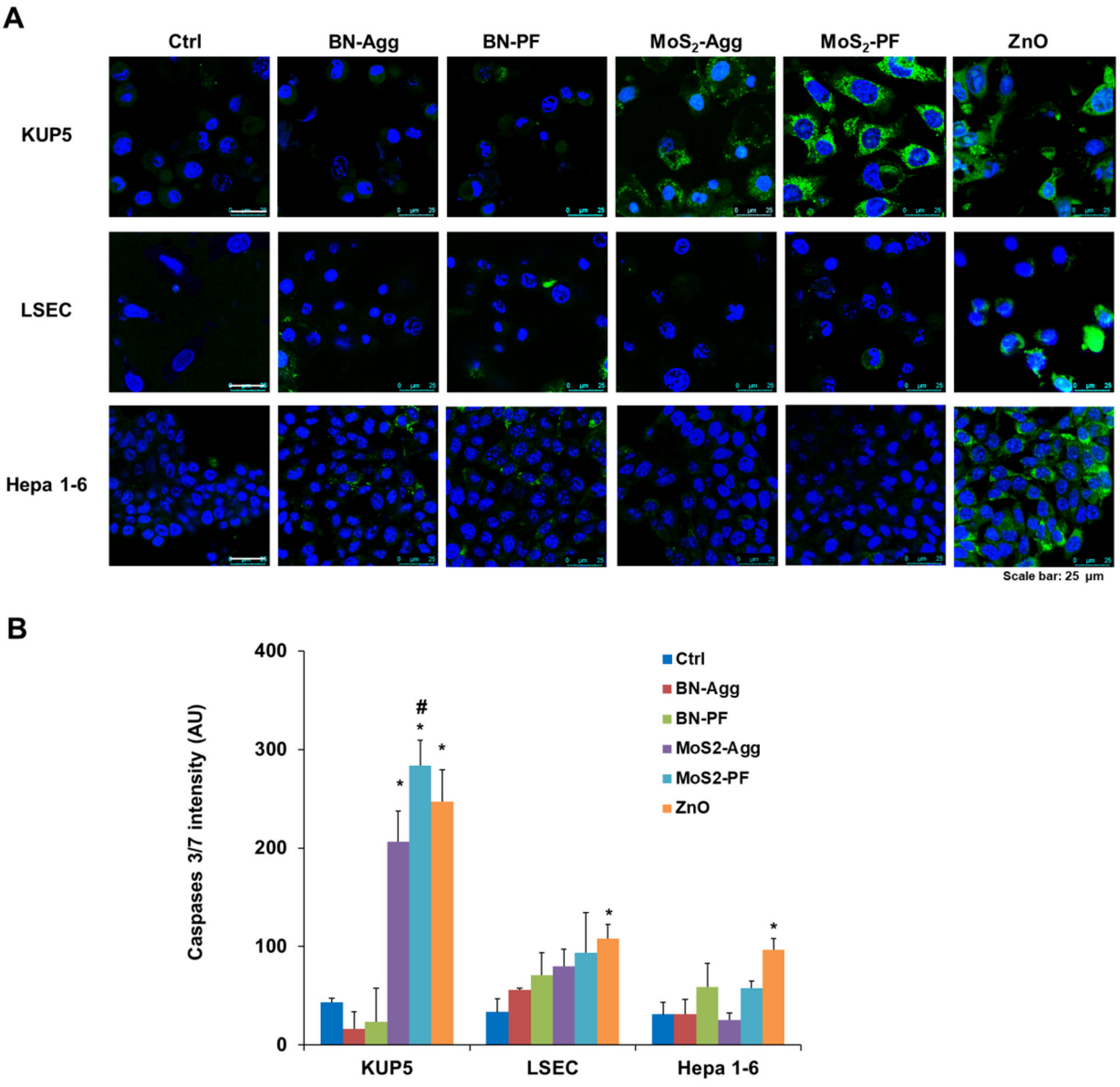

Figure 6. Assessment of apoptotic cell death in the liver cells.

(A) Confocal images to determine caspase 3/7 activation by BN and MoS_2 nanosheets in KUP5, LSEC, and Hepa 1–6 cells. Cells were exposed to 25 μg/mL of the materials for 16 h, before staining with the FAM-FLICA caspase 3/7 substrate (green) for 1 h and Hoechst 33342 (blue) for 15 min. ZnO was used as a positive control. The scale bar represents 25 μm. (B) Quantification of caspase activation in a microplate reader. The fluorescence intensity was monitored at excitation/emission wavelengths of 492/520 nm. *, $p < 0.05$ to show the significant difference from the untreated control; #, $p < 0.05$ denotes a significant difference between MoS_2-Agg and MoS_2-PF.

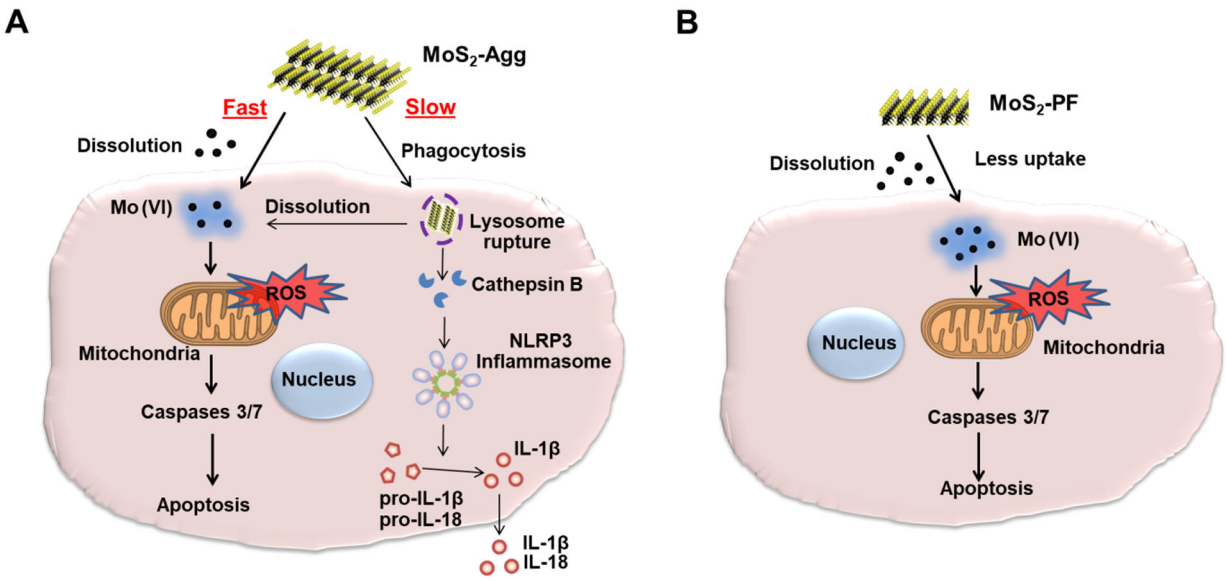

Figure 7. Schematics to outline the contribution of aggregation status *vs.* the dissolution of MoS_2 in KUP5 toxicity.

(A) Schematic to show the contribution of MoS_2-Agg to material toxicity by material dissolution to generate cytotoxicity through ROS generation, caspase 3/7 activation, and apoptotic cell death. In addition, phagocytosis of MoS_2-Agg triggers lysosomal damage, cathepsin B release, caspase-1 activation, and IL-1β production, without pyroptosis. (B) Schematic of the mechanism of toxicity of MoS_2-PF, a well-dispersed material with a high dissolution rate, leading to the release of Mo (VI), and induction of apoptosis, as explained in panel A.

Table 1.

Quantification of BN composition as determined by XPS.

Sample	BN-Agg	BN-PF
B-N %	49.5 ± 1.3	48.6 ± 1.2
B-O %	5.9 ± 1.2	6.3 ± 1.3
N-B %	37.3 ± 1.0	39.5 ± 1.7
N-H %	7.3 ± 1.2	5.7 ±1.4
N: B Ratio	0.81 ± 0.0	0.82 ± 0.0

Table 2.

Quantification of MoS_2 composition as determined by XPS.

Sample	MoS_2-Agg	MoS_2-PF
Mo (IV) 3d%	36.3 ± 1.0	32.7 ± 0.9
Mo (VI) 3d%	3.3 ± 0.8	10.2 ± 1.4
S At. %	60.4 ± 0.3	57.1 ± 0.8
S: Mo Ratio	1.52 ± 0.0	1.30 ± 0.2

Table 3.

Hydrodynamic size, polydispersity index (PDI), and zeta potential of BN and MoS2 in different media.

Media	Sample	Hydrodynamic size (nm)	PDI	Z-potential (mV)
DI water	BN-Agg	1219.2 ± 59.2	0.385 ± 0.009	−16.9 ± 1.0
	BN-PF	134.0 ± 0.2	0.172 ± 0.006	−24.6 ± 1.1
	MoS_2-Agg	730.9 ± 36.3	0.319 ± 0.016	−31.9 ± 1.4
	MoS_2-PF	92.5 ± 0.6	0.265 ± 0.010	−19.9 ± 2.3
DMEM (KUP5)	BN-Agg	1299.5 ± 56.7	0.327 ± 0.046	−10.3 ± 2.6
	BN-PF	202.5 ± 2.0	0.125 ± 0.033	−12.1 ± 4.5
	MoS_2-Agg	883.3 ± 24.9	0.356 ± 0.011	−11.1 ± 1.2
	MoS_2-PF	106.9 ± 1.5	0.244 ± 0.007	−10.3 ± 1.0
Prigrow medium (LSEC)	BN-Agg	1323.6 ± 44.9	0.358 ± 0.038	−9.0 ± 3.5
	BN-PF	175.6 ± 1.3	0.136 ± 0.008	−11.3 ± 0.4
	MoS_2-Agg	813.2 ± 13.2	0.331 ± 0.009	−11.9 ± 5.6
	MoS_2-PF	99.5 ± 1.8	0.256 ± 0.011	−10.5 ± 0.3
DMEM (Hepa 1–6)	BN-Agg	1245.6 ± 56.8	0.371 ± 0.024	−11.8 ± 5.0
	BN-PF	189.3 ± 3.6	0.162 ± 0.005	−10.2 ± 2.6
	MoS_2-Agg	847.6 ± 25.2	0.340 ± 0.018	−12.8 ± 2.3
	MoS_2-PF	98.6 ± 0.5	0.257 ± 0.023	−7.2 ± 0.6